Aligned PVDF-TrFE Nanofibers With High-Density PVDF Nanofibers and PVDF Core–Shell Structures for Endovascular Pressure Sensing

Tushar Sharma*, Sahil Naik, Jewel Langevine, Brijesh Gill, and John X. J. Zhang

***Abstract*—Nanostructures of polyvinyledenedifluoride-tetrafluoroethylene (PVDF-TrFE), a semicrystalline polymer with high piezoelectricity, results in significant enhancement of crystallinity and better device performance as sensors, actuators, and energy harvesters. Using electrospinning of PVDF to manufacture nanofibers, we demonstrate a new method to pattern high-density, highly aligned nanofibers. To further boost the charge transfer from such a bundle of nanofibers, we fabricated novel core–shell structures. Finally, we developed pressure sensors utilizing these fiber structures for endovascular applications. The sensors were tested *in vitro* under simulated physiological conditions. We observed significant improvements using core–shell electrospun fibers (4.5 times gain in signal intensity, 4000 μV/mmHg sensitivity) over PVDF nanofibers (280 μV/mmHg). The preliminary results showed that core–shell fiber-based devices exhibit nearly 40-fold higher sensitivity, compared to the thin-film structures demonstrated earlier.**

***Index Terms*—Core–shell, catheter, nanofibers, polyvinyledenedifluoride-tetrafluoroethylene (PVDF-TrFE), pressure sensor.**

I. Introduction

MINIMALLY invasive surgeries have emerged as the cornerstone for the diagnosis and treatment of cardiovascular diseases. Minimally invasive surgeries typically employ catheters, which still rely on fluid-filled lumen coupled with an external transducer, for endovascular pressure measurements [2]–[4]. Such fluid-filled catheters have inherent inaccuracies related to resonance in the system. The resonance is a function of the length and diameter of the tubing and the frequency of the waveform being measured, which is typically the heart rate for intravascular systems [5]. There has been great effort dedicated to the development of silicon microelectromechanical systems (MEMS) based pressures sensors [6], [7]. Though MEMS pressure sensors currently dominate the market for greater-than-atmospheric-pressure measurement systems, they have had limited success in the minimally invasive catheter-based pressure sensing arena. With the increasing demands of quality and reliable data in real time, development of such "smart catheters" integrated with compact, flexible, and high-performance pressure sensors with proven biocompatibilities are critical.

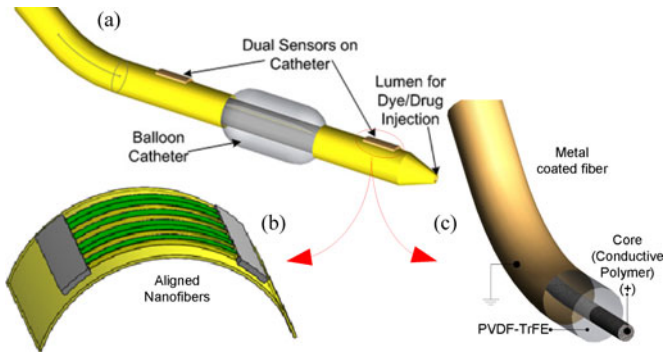

Fig. 1. Smart catheters with nanofiber-based pressure sensors. (a) Placement of pressure sensors on either side of balloon on a catheter; (b) highly aligned nanofibers-based pressure sensor; (c) core–shell fiber showing the sandwiched layers of piezoelectric polymer.

Flexible piezoelectric materials are emerging as a promising solution for developing a new class of pressure sensors mounted on a single catheter [see Fig. 1(a)] with desirable form factors, sensitivities and locations for measurements. The use of piezoceramics, such as ZnO and PZT, has been limited due to concerns of biocompatibility and brittleness, but piezoelectric polymers have shown tremendous growth as the key materials for biosensors [1], [8]–[16]. Polyvinyledenedifluoride (PVDF) has been conventionally drawn in to films either by melt casting or solvent casting. However, nanostructures made out of PVDF showed enhanced piezoelectricity [17], [18]. Previously, we reported the fabrication of 1-μm-thick film and showed enhanced sensing capabilities compared to thicker films [1], [8]. In this study, we report further enhancement in the sensing capabilities by employing high density of highly aligned nanofiber-based structures [see Fig. 1(b)].

To fabricate regular PVDF and PVDF core–shell nanofibers on a substrate, we employ and optimize the technique of electrospinning in this study. Electrospinning is a process through which nanofibers are produced under the influence of an electric

Manuscript received August 23, 2013; revised May 26, 2014; accepted July 19, 2014. Date of publication July 30, 2014; date of current version December 18, 2014. *Asterisk indicates corresponding author.*

*T. Sharma was with Biomedical Engineering Department, Center for Nano and Molecular Science, The University of Texas at Austin, Austin, TX 78712 USA. He is now with Intel Corporation , Hillsboro, OR 97124 USA (e-mail: tusharsharma@utexas.edu).

S. Naik and J. Langevine are with Biomedical Engineering Department, The University of Texas at Austin, Austin, TX 78712 USA (e-mail: sahil.naik@utexas.edu; jewel.Langevine@utexas.edu).

B. Gill is with the University of Texas Health Science Center at Houston, Houston, TX 77026 USA (e-mail: billy@empowerment.com).

J. X. J. Zhang was with Biomedical Engineering Department, Center for Nano and Molecular Science, The University of Texas at Austin, Austin, TX 78712 USA. He is now with, Dartmouth College, Hanover, NH 03755 USA (e-mail: john.zhang@dartmouth.edu).

This paper has supplementary downloadable material available at http://ieeexplore.ieee.org.

Color versions of one or more of the figures in this paper are available online at http://ieeexplore.ieee.org.

Digital Object Identifier 10.1109/TBME.2014.2344052

field (see Figure S1a, available in the online supplementary material). Previously, it has been shown that the higher strain gradients and higher electromechanical coupling coefficients associated with nanofibers can result in significantly higher signal output compared to PVDF thin films [12]. However, most of the studies involved testing of few microfibers only [17], [19]. Increasing the density of aligned fibers is crucial for enhancing sensor performance, which has been a hindrance in the field of electrospinning. This challenge is mainly due to the difficulty in fabricating high density of highly aligned electrospun fibers [20]–[23]. Here, we analyze and present a way to electrospin high density of highly aligned nanofibers [see Fig. 1(b)].

Aligned-nanofiber-based devices tap into the high electromechanical coupling coefficients to generate higher signal output. Therefore, fabrication of high density of highly aligned nanofibers can help further increase the signal output. However, aligned-nanofiber-based sensors call for extra steps to prevent the effect of stray electrostatic charges interfering with device signals. Further, most of the usable charge is lost due to the high internal resistance of the PVDF polymer. Therefore, using aligned nanofibers is not the most ideal scenario.

In order to circumvent the aforementioned problem, we also report fabrication of core–shell fibers [see Fig. 1(c)]. The core of this fiber is composed of conductive polymer (PEDOT:PSS), acting as one of the electrodes. The shell, comprising PVDF-tetrafluoroethylene (PVDF-TrFE), was co-electrospun with the conductive core polymer to fabricate core–shell fibers. After successful patterning of core–shell structures, a thin film of metal was deposited to form the external electrode. High sensitivity can be expected from these devices due to a larger surface area being in contact with the PVDF polymer. To the best of our knowledge, application of core–shell fibers for sensing application has not been explored. Development of versatile sensors that use core–shell structures can profoundly revolutionize the pressure sensing application in catheter development.

II. Experimental Section

A. Electrospinning for High Density of Highly Aligned Nanofibers

Electrospinning is the most popular way to produce ultrathin polymeric nanofibers [24]–[28]. The process involves subjecting a polymer solution held at the needle tip by its surface tension, to an electric field. The high electric fields involved in electrospinning results in substantial charge accumulation to be able to overcome the surface tension. As the intensity of the electric field increases, the solution at the tip of the needle elongates to result into a conical shape known as the Taylor's cone [24]–[26], [29]. As the electric field is further increased, the electric field reaches a critical value at which the repulsive electric force overcomes the surface tension force, resulting in a jet of solution that gets deposited on the ground collector plate.

In the electrospinning of polymer solutions, a number of parameters are known to affect the physical properties of the fibers, including the fiber shape, diameter, surface morphology, and porosity [17].

1) Setup: The electrospinning setup consisted of a solution-filled syringe on a syringe pump whose needle was connected to an external high voltage (see Figure S1, available in the online supplementary material). Across the tip of the needle, a collector plate or electrode was placed at a certain distance, which was connected to the ground of the external high voltage supply. Figure S1b (available in the online supplementary material) shows the actual setup used for electrospinning of fibers in this study with a copper plate (ground collector) placed 7 cm away from the needle tip inside an acrylic box. The acrylic box was used to prevent electrostatic charging of the surroundings.

2) Parameter Optimization: There are multiple variables in an electrospinning setup that need to be optimized in order to fabricate uniform fibers. Details on optimized variables for electrospinning of PVDF solution has been discussed elsewhere [30]. In brief, PVDF concentration of 5%–20% (w/v) was used. Methyl ethyl ketone (MEK) was used as the primary solvent for electrospinning of PVDF nanofibers. Preliminary fabrication of nanofibers was done on ground copper plate as the electrode (see Fig. 3). Mesh (stainless steel) electrodes offered better control over the fiber orientation [30]. A voltage gradient of 1–3 kV/cm was used with the needle tip–collector distance being greater than 7 cm.

3) Rotating Drum Electrodes: Most of the studies on aligned nanofibers have reported the use of a rotating drum so far [20], [23], [25]. Conventionally, the entire rotating drum would be grounded and the nanofibers would be deposited on the drum in an aligned fashion because of the high rotating speeds of the drum. In this study, we initially started with such a rotating drum setup by grounding the entire rotating drum. However, lack of capability to fabricate high density of aligned nanofibers led up to optimize the rotating drum geometry.

The present version of the rotating drum setup is shown in Figure S2 (available in the online supplementary material). The drum itself is constructed out of an ABS-like plastic, using a laser sintering machine. The diameter of the rotating drum is 1.2 in (30.5 mm), and the length of the drum was 3.5 in (89 mm). Grounded copper wires (3-mm diameter) were connected to the ground wire, which was passed through the hollow shaft and connected to external ground near the rotating motor holder. The entire assembly, comprising motor holder and the rotating drum holder, was also fabricated using the same laser sintering machine. The dc motor powering the rotating drum was controlled through an external power supply and the rotational speed could be controlled in the range of 0–4000 r/min. Typically, a Kapton film was rolled over the rotating drum assembly for the patterning of aligned nanofibers.

B. Core–Shell Electrospinning Process

To electrospin core–shell nanofibers, the solution dispensing mechanism was altered slightly, such that it allowed concomitant flow of two solutions with the shell solution encapsulating the core solution, as shown in Fig. 2. Figure S3 (available in the online supplementary material) shows the schematic of the modified setup and a photograph of the actual setup.

For core–shell electrospinning, the needle-in-needle assembly was optimized such that the inner needle was perfectly

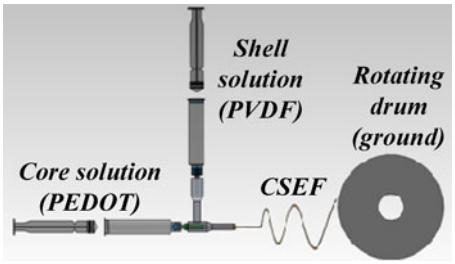

Fig. 2. Schematic of the core–shell electrospinning setup along with the rotating drum (front view).

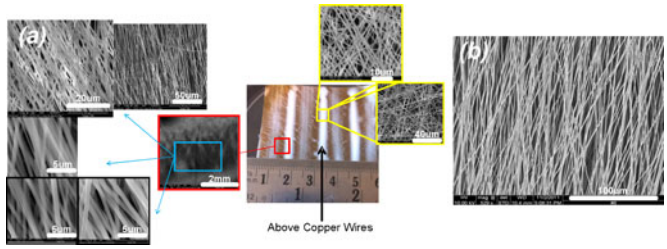

Fig. 3. (a) Photograph and SEM images showing patterned nanofibers in aligned and random orientations; and (b) SEM image of a high-density, highly aligned fiber sample fabricated using the rotating drum setup for 45 min.

aligned, concentrically to the outer needle. Further, the whole two-needle assembly was made airtight to avoid any leakages and evaporation of PVDF solvent. The tip of inner needle was slightly protruding from the tip of the outer needle. The core and shell solutions were kept at flow rates of 1 and 3 mL/h, respectively. The core solution was prepared by mixing 1.6 g of (poly(3,4-ethylenedioxythiophene) poly(styrenesulfonate) (PEDOT:PSS, 2% in water, Sigma Aldrich) with 0.2 g of polyvinylpyrrolidone (PVP) in 5 g of dimethylformamide (DMF). Rhodamine B (0.1%, w/v, Sigma Aldrich) dye was added for fluorescence. The shell solution contained 14% (w/v) of PVDF-TrFE powder (70:30) dissolved in DMF-MEK (25:75). 1-Pyrenebutyric acid (0.2%, w/v, Sigma Aldrich) dye was added to the shell solution for fluorescence imaging.

To measure the resistance of the core-material that was used to fabricate core–shell structure, we employed a simple testing setup. Two silver wires (1.5 mm diameter, 99.99% pure, Alfa Aesar) were wrapped around a glass slide, separated by a gap of 1 cm. This glass slide was pressed against the testing sample on another glass slide. The two silver wires were then connected to an external digital multimeter to measure the sample resistance, and the sample conductivity was calculated using the following:

$$S = \frac{1}{Rtw}$$

where S is the conductivity of the samples (in S/cm), l is the separation between silver wires (1 cm), t is the thickness of sample, w is the width of sample, and R is the resistance of the sample (in ohms).

C. Device Assembly

The devices had a functional surface area of 10×4 mm^2, as shown in Figure S6a (available in the online supplementary material). To fabricate flexible devices, metal electrodes were patterned on Kapton (polyimide) film. A copper (350 nm) metal electrode was deposited using photoresist lift-off followed by e-beam deposition. The patterned Kapton film was wrapped around the rotating drum setup and nanofibers were directly electrospun on top. In order to connect the PVDF shell material to the other electrode, copper metal was e-beam deposited from top (350 nm) using a hard shadow mask. Electrical wires were connected to the electrode pads using silver paint. The devices were spin coated with UV curable epoxy (NOA 89) for external passivation. After device assembly, the devices were placed either in the fluid testing chamber or the vascular testing model for further testing. The detailed protocols for device testing and the associated circuitry are reported elsewhere [1], [31]. The results obtained from PVDF sensors were compared against commercial pressure sensor (Freescale semiconductors, MPX2300DT1), fitted in the same testing setup.

III. Results

A. Highly Aligned Nanofibers

Figure S2 (available in the online supplementary material) shows the rotating drum setup in the holder, and Fig. 3 shows the images of the fabricated nanofibers. Electrospinning of fibers for 20 min yielded aligned fibers with an average diameter of 737 ± 75 nm [see Fig. 3(a)].

It was generally found that the highly aligned nanofibers stretch in the area between the two ground copper wires. The portion of substrate directly above the copper wires was found to have randomly oriented nanofibers [see Fig. 3(a)]. A similar effect has also been reported before [22].

To fabricate a high density of highly aligned nanofibers, electrospinning was carried out for longer time duration (45 min). The results, as shown in Fig. 3(b), indicates high density of highly aligned nanofibers with an average diameter of 963 ± 86 nm. For all subsequent experiments, electrospinning was carried out for 45 min.

For a better understanding behind the high alignment of the fibers using rotating drum assembly, we quantified the fiber alignment based on the protocol described in [32]. Since the described protocol was for quantification of fiber alignment from optical microscopy images, we altered the protocol that it was more suitable for SEM (Scanning Electron Microscope) images and takes into account the variations in illumination and charging effects. The modified protocol is shown in Figure S4 (available in the online supplementary material). In order to process the images using this protocol, we used ImageJ (NIH) along with the Oval profile intensity plug-in. In this study, we did not rotate the fast Fourier transform (FFT) image by 90° to account for the shift in angle. The oval profile plug-in allowed plotting the total sum of gray pixel intensities along the blue line (see Figure S4, available in the online supplementary material) for a sweeping angle of 0–360°.

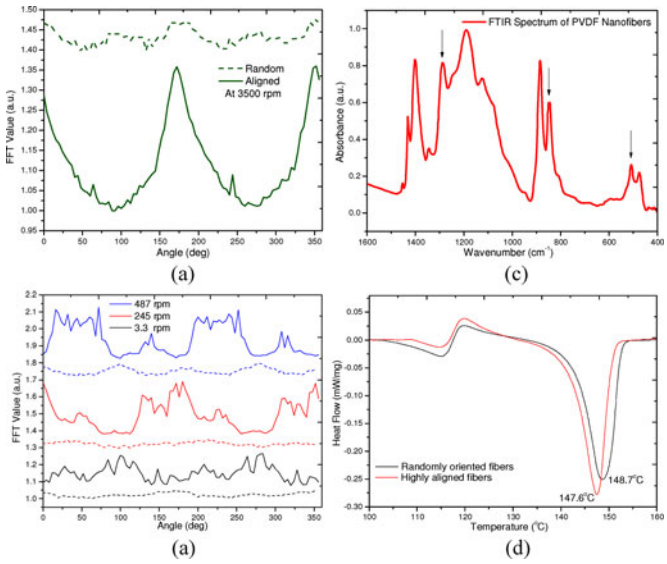

Fig. 4. Characterization of nanofiber alignment, using plots of oval profile intensity for (a) aligned and random portion of fibers electrospun at 3500 r/min; (b) aligned (PVDF) and random (dashed) portion of fibers at different speeds of rotating drum; (c) FTIR spectrum of electrospun PVDF nanofibers; and (d) characterization of crystallinity, using weight-normalized DSC curves for aligned and randomly oriented nanofibers patterned on Kapton substrate.

Using the aforementioned technique, we studied the effect of fiber alignment due to variation in rotating drum speeds (for 3.3, 245, 487, and 3500 r/min). Figure S5 (available in the online supplementary material) shows the SEM images obtained from different parts of the rotating drum for varying speeds of the drum. All the fiber alignment studies were carried out for 20 min using 14% (w/v) PVDF solution in MEK. From the SEM images in Figure S5, we observe that with the increase in speed of the rotating drum, the density of fibers that are aligned increases correspondingly. Whereas the density of the fibers deposited directly above the ground copper wires (randomly oriented fibers) decreases for increasing rotating drum speeds. Each SEM figure was processed as per the method described in Figure S4 (available in the online supplementary material) and the corresponding two-dimensional (2-D) FFT images obtained for each SEM image has been presented in Figure S5 (available in the online supplementary material).

Results of using oval intensity plot on the 2-D FFT images have been summarized in Fig. 4. Fig. 4 compares the FFT value (gray pixel intensity summation) as a function of the angle sweep. All the curves were normalized to the lowest FFT value in the intensity plot. The individual plots were shifted for ease of comparison.

From Fig. 4(a), we notice that aligned fiber intensity plots has two peaks in a 0°–360° intensity plot. Presence of two peaks, separated by an angle of 180° indicates aligned fibers, represented by the periodicity in the 2-D FFT plots [32].

On the other hand, randomly oriented nanofibers are expected to show four peaks over the same range of 0–360° intensity plot [32]. From Fig. 4(a), we clearly see this trend. Further, the presence of two dominant peaks is a good indication of highly aligned nanofibers. Increase in the drum rotation speed results in better alignment of nanofibers. Furthermore, it was found that the amplitude of the intensities of randomly oriented nanofibers was much lower compared to those of aligned nanofibers. This difference in the amplitude could be easily used as key parameter to distinguish between aligned and randomly oriented nanofibers. On similar lines, Fig. 4(b) shows that as the rotating drum speed is increased, the fibers tend to align better, indicated by the diminishing amplitude of the peaks and emerging prominence of two peaks at higher rotation speeds. However, the randomly oriented nanofibers [see dashed curves in Fig. 4(b)] do not show appreciable change in nanofiber orientation.

Fig. 4(c) shows the Fourier transform infrared (FTIR) spectrum obtained from electrospun fibers on a 4-in silicon wafer coated with copper. Coated silicon wafer was used as the substrate because grazing angle incidence in reflectance mode was used for spectroscopy. The FTIR spectrum was obtained for eight different spots on the wafer in grazing angle incidence mode and then averaged to obtain the curve shown in Fig. 4(c). A quick comparison of the FTIR spectrum of electrospun fibers with previously reported FTIR curves [1], [8] indicates the presence of high beta crystal phase in nanofibers.

Fig. 4(d) shows the DSC (Differential Scanning Calorimetry) curves obtained for nanofiber samples. Highly aligned nanofibers (14%, w/v, PVDF/MEK) were patterned on fluoropolymer substrate (ACLAR, Electron microscopy sciences) as detachment of fibers was much more easily compared to fibers electrospun on Kapton film. From Fig. 4(d), we infer that the aligned nanofibers show slightly higher crystallinity compared to randomly oriented nanofibers. However, the increase in crystallinity was insignificant.

B. Core-Shell Nanofibers

For the sensor applications of the core–shell nanofiber structure, it is crucial to design and fabricate a conductive core acting as one of the electrode. Gold nanoparticles have been used for fabrication of conductive nanofibers [33]. We initially employed the use of silver nanoparticles (20–40 nm, Alfa Aesar) mixed with poly(methyl methacrylate (PMMA, 15% w/v) in DMF as the solvent. However, the resistance of fibers electrospun using silver nanoparticles was very high (greater than megaohms).

In place of metallic nanoparticles as additives, conductive polymers offered a better alternative. Some of the common conducting polymers include polyaniline (PANI) and PEDOT:PSS. PANI, by itself, is very conductive but grainy, which can easily clog the electrospinning needle. Filtered PANI, however, is not as conductive even when doped with CSA (10-camphorsulfonic acid) or prepared in *m*-cresol as the primary solvent (see Table S1, available in the online supplementary material). From Table S1 (available in the online supplementary material), we found that PEDOT:PSS in water gives similar conductivity, comparable to PANI doped with CSA in *m*-cresol solution (unfiltered). Further, PEDOT solution was not grainy like PANI, making it suitable for electrospinning.

For imaging of the core–shell fibers fabricated, we employed TEM imaging. Fig. 5 shows the TEM images of all the core–shell fibers electrospun directly on the rotating drum setup. TEM imaging was highly suitable for imaging of core–shell fibers of

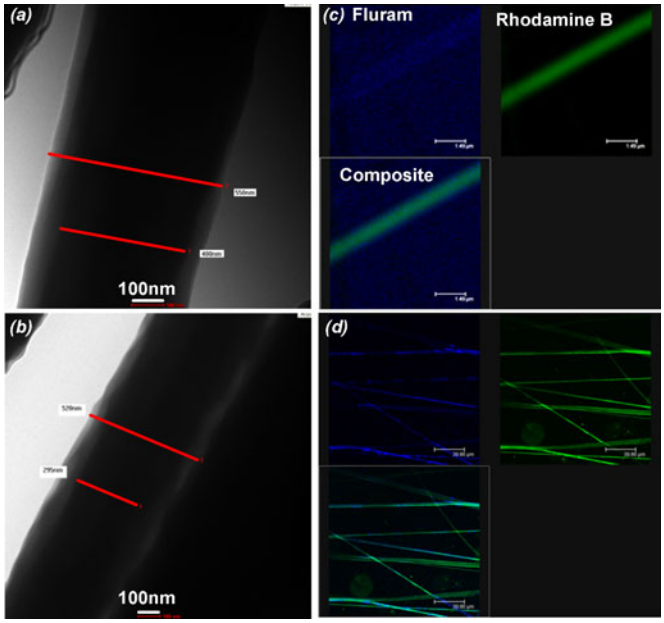

Fig. 5. CSEFs. (a) and (b) TEM images. (c) and (d) Confocal laser fluorescence microscopy images. Labeling: Rhodamine B for the core (PEDOT) and Fluram for the shell (PVDF).

couple hundred nanometers thickness. The darker core is visible in most of the fibers.

However, TEM could not be used to image fibers thicker than 500 nm. For thicker fibers, confocal imaging using selectively dyed materials was used to visualize core–shell fibers. Table S2 (available in the online supplementary material) summarizes the various fluorescent dyes and their characteristics, used in this study.

The best dye combination was observed with Rhodamine B (core) and 1-pyrenebutyric acid or Fluram (shell). Fig. 5 shows confocal laser fluorescence microscopy images of core–shell fibers electrospun directly on to a rotating drum assembly for patterning highly aligned core–shell fibers. From the images, we observe good percentage of core–shell fibers present, shown by simultaneous fluorescence of Fluram and Rhodamine B. Better core–shell fibers were observed either by: 1) electrospinning without dyes and with MEK as the only shell solvent (see Figure S3, available in the online supplementary material), or 2) electrospinning larger diameter fibers (see Figure S3, available in the online supplementary material).

FTIR spectroscopy was used to detect presence of PEDOT and PVP in core–shell electrospun fiber (CSEF). While a PVDF spin-coated layer on top of a PEDOT layer shows presence of PEDOT (see Fig. 6), core–shell fiber spectrum was similar to electropsun PVDF fiber mat (indicated by arrows pointing to beta phase wavenumbers). FTIR spectrum of CSEF mat at various incident points yielded the same spectrum, indicating that the PEDOT core fiber was very thin for sufficient absorption of signal. This was also a good indicator of presence of core–shell fibers, in place of formation of co-spun fibers or splitting of Taylor's cone leading to electrospinning of just PEDOT fibers on the surface.

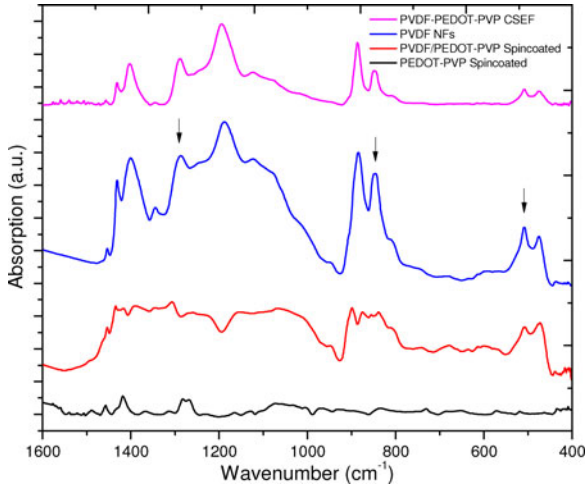

Fig. 6. FTIR spectrum obtained from CSEFs, in comparison with that of spin-coated PEDOT-PVP mixture and PEDOT film, randomly oriented PVDF nanofibers, and a layer of PVDF spin coated on top of PEDOT-PVP layer.

C. Device Setup

Figure S6 (available in the online supplementary material) shows the various stages in the device assembly. The open-circuit resistance of the final devices was found to higher than 1 GΩ (measurable limit of the digital multimeter). In order to connect the conductive core to the electrode collector, silver paint was used along the length of the electrode (see Figure S6b, available in the online supplementary material). Silver paint contains organic polar solvents, which help dissolve the PVDF-TrFE coating and establish a conductive connection to the core PEDOT-PVP fiber. Control experiments were done where both the electrodes were covered with silver paint to short circuit the devices and the resistance of the devices fell to 1.5 MΩ, which also happened to be the resistance of a bulk (spin-coated) PEDOT-PVP film (1 cm length). This is an indication of good connectivity of the core fiber with the electrode pad.

Following the connection of the core using silver paint and shell using copper, the resistance between the two electrodes was found to be greater than 1 GΩ, indicating good isolation of core–shell electrodes and corresponding electrical connections.

D. Testing Results

Figure S7 (available in the online supplementary material) compares the performance of random nanofiber-based devices alongside the performance of aligned nanofiber-based devices. Both the sensitivity plots show the device performance at 30 dB. From the sensitivity plots, we notice that aligned-nanofiber-based devices show higher sensitivity (280 μV/mmHg) compared to the random nanofiber-based devices (65 μV/mmHg) at 30 dB of amplification at the charge amplifier. Further, the aligned-nanofiber-based devices showed better linearity, indicated by the higher residual sum of squares value.

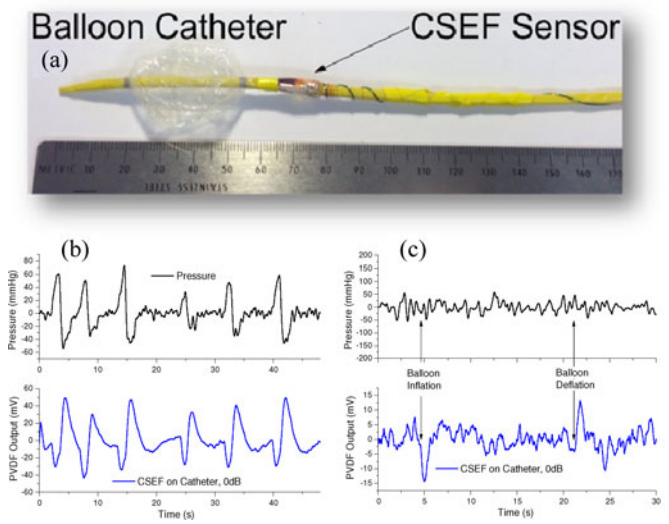

Fig. 7. Performance of CSEF-based sensor mounted on the catheter. (a) Schematic of the smart catheter prototype; (b) performance of a CSEF device mounted on catheter surface compared against the commercial pressure sensor; (c) response obtained from CSEF-based sensors on catheters upon inflation and subsequent deflation of a balloon on catheter, compared against no signal received from the commercial pressure sensor.

For catheter assembly, a commercial aortic occlusion catheter was used for testing (10Fr gauge, Coda Aortic Catheter, Cook Medical, Bloomington, IN, USA). A pair of 40-gauge insulated magnetic wires was used to make connections to the device electrode pad. The electrical wires were wrapped around the catheter surface or passed through the internal lumen space of the catheter [see Fig. 7(a)]. The electrical connection was made using silver paint. The whole joint was insulated using UV-curable epoxy.

Fig. 7 shows a comparison between the commercial pressure sensor and high quality response obtained from the CSEF-based sensors that were mounted on a catheter. Fig. 7 shows the raw signal obtained from the PVDF sensor without any amplification. From Fig. 7, PVDF sensor showed good correlation with water pressure inside the testing chamber. The PVDF sensor was sensitive enough to detect balloon deflation as well, which was not detected by the commercial pressure sensor. The average response time of the PVDF sensors (0.26 s) was found to be five times faster than the commercial pressure sensor (1.30 s) when evaluated for the 0%–100% pressure change. Fig. 7(c) shows the same device response obtained when the balloon was inflated and deflated.

Only the CSEF-based sensor was capable of detecting the pressure variations due to the changes in balloon condition and any change in the system went unnoticed by the commercial pressure sensor. This was due to the shorter response time of the PVDF sensor, whereas instantaneous pressure changes go unnoticed by the commercial pressure sensor.

Fig. 7 shows the performance of CSEF-based devices plotted at 0 dB. The core–shell-based devices showed high sensitivity (4 mV/mmHg) along with high linearity ($\mathrm{R-value} = 0.99$) over the required pressure range of 0–300 mmHg. The average fiber diameters for CSEFs tested in this study were 1 μm (see Figure S8, available in the online supplementary material).

IV. Discussions

As reported before [30], PVDF concentration has the highest impact on the fiber diameter, as compared to the solution flow rate or needle gauge diameter. Further, using the mesh-based current collector electrode, high density of nanofibers can be easily achieved by increasing the electrospinning time. It was difficult to obtain highly aligned nanofibers, however. Rotating-drum assembly resulted in high density of highly aligned nanofibers [30].

In order to find out the variability between different samples of highly aligned electropsun fibers, three different electrospinning samples were analyzed for fiber alignment and diameter distribution. All the variables, including electrospinning time, voltage gradient, and drum rotation speed, were maintained constant. Figure S9 (available in the online supplementary material) summarizes the fiber distribution over the three different samples fabricated. We observed similar fiber diameters and fiber count distribution for two of the three different samples electrospun. Therefore, it is possible to control fiber diameters reliably over large number of samples by keeping the electropsinning variables constant.

The aligned-nanofiber-based devices showed higher sensitivity (280 μV/mmHg, scaled to 40 dB) compared to the thin-film-based devices (99 μV/mmHg at 40 dB [1]) while at the same time using only half the piezoelectric material (estimated from the average fiber diameter and surface fiber density). This high sensitivity was also capable of detecting minor fluctuations in the flow rates (see Figure S10, available in the online supplementary material), where the commercial pressure sensor failed to show any minor pressure variations. Figure S11 (available in the online supplementary material) indicates that the signal was obtained due to the piezoelectricity of the nanofibers, rather than external electrostatic charges. Preliminary studies showed insignificant impact on the sensor sensitivities due to temperature variations (see Figure S12, available in the online supplementary material).

For the electrospinning of core–shell fibers, switching from the horizontal electrospinning to vertical setup aided in the ease of electrospinning and formation of a good Taylor's cone with the help of gravity. Increasing the electrospinning distance also helped in formation of thinner, complete fibers. Electrospinning at shorter distance ($<$10 cm) did not allow all the solvent to evaporate and resulted in formation of flatter fibers. However, the Taylor's cone would solidify quickly, leading to discontinuous electrospinning of CSEF. Therefore, the shell solvent was changed from purely MEK based to a mixture of MEK and DMF (75:25 ratio). Addition of DMF to the solvent mixture increased the effective boiling point and allowed more time for the PVDF to remain in dissolved state. These series of optimizations enabled fabrication of core–shell fibers with good consistency and controlled patterning.

In order to have PVDF polymer as the shell for CSEF, polymers that were soluble in organic solvent were used. Hence,

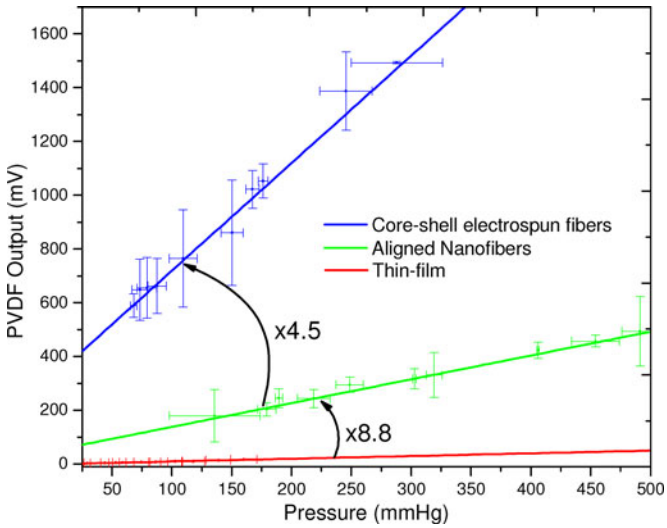

Fig. 8. Sensitivities of various sensors based on CSEFs, aligned PVDF nanofibers, and thin-film PVDF sensors fabricated in this study.

PMMA and PVP were used as the suitable polymers for forming core materials. However, in order to successfully fabricate pressure sensors from core–shell nanofibers, it is necessary to have a conductive core that is capable of transferring the charge generated from PVDF-TrFE to the terminal conducting electrode. PEDOT-based core fibers were promising for such an application. PEDOT was found to be more conductive compared to PANI (see Table S1, available in the online supplementary material) and was more readily electrospinable as PEDOT did not have granular structure like PANI. An important test was to ensure that the signal obtained from CSEF-based devices was due to the piezoelectricity from the samples, rather than the instrumentation. Figure S13 (available in the online supplementary material) indicated a strong presence of piezoelectricity from core–shell electrospun nanofibers, observed by change in device polarity on swapping of electrode connections.

The core–shell-based devices showed good performance that was 4.5 times higher than the aligned nanofiber-based devices (see Fig. 8). Fig. 8 summarizes the performance comparison of the various transducer designs fabricated in this study. We clearly see 8.8 times higher signal output from nanofiber-based devices than from the thin-film-based devices, which in the same range of electromechanical efficiency enhancement as reported previously for nanofibers versus thin-film-based devices [17]. The noise from the sensors can be further reduced by an additional thin metallic film that prevents the effect of any external electrostatic charges.

V. Conclusion

In summary, we successfully demonstrated that patterning of high density, highly aligned PVDF-TrFE nanofibers is possible using a high-speed rotating drum. We validated the alignment of the fibers quantitatively using 2-D FFT of the SEM images. We also demonstrated the ability to fabricate highly aligned nanofibers with crystallinity similar to those of thin films we developed previously [1], [8], with additional advantages of significantly boosted device sensitivity by virtue of higher flexibility and lower material consumption. We also developed CSEFs with a conductive core. PVDF-TrFE is an extremely robust material with suitable biocompatibility for sensing applications. A series of pressure sensor prototypes were developed based on the nanofibers and characterized in fluid-filled chambers. We observed significant improvements using CSEFs (4.5× gain, 4000 μV/mmHg sensitivity) over PVDF nanofibers (280 μV/mmHg). Flexible nanofibers has shown great promises for the realizations of more robust, reliable, flexible pressure sensors on catheters to revolutionize the field of minimally invasive surgeries.

References

[1] T. Sharma, T. K. Aroom, S. Naik, B. Gill, and J.X.J. Zhang, "Flexible thin-film PVDF-TrFE based pressure sensor for smart catheter applications," *Ann. Biomed. Eng.*, pp. 1–8, 2012.

[2] Å. Kjällquist, N. Lundberg, and U. Ponten, "Respiratory and cardiovascular changes during rapid spontaneous variations of ventricular fluid pressure in patients with intracranial hypertension," *Acta Neurol. Scand.*, vol. 40, no. 3, pp. 291–317, 1964.

[3] N. Lundberg, "Continuous recording and control of ventricular fluid pressure in neurosurgical practice," *Acta Psychiatr. Scand.*, vol. 36, no. 149, p. 1, 1960.

[4] J. Miller and J. Pickard, "Intracranial volume/pressure studies in patients with head injury. injury," vol. 5, no. 3, pp. 265–269, 1974.

[5] K.D. Wise and J. B. Angell, "An IC piezoresistive pressure sensor for biomedical instrumentation.," *IEEE Trans Biomed Eng.*, vol. 2, pp. 101–109, 1973.

[6] R. C. Ostrup, T. G. Luerssen, L. F. Marshall, and M. H. Zornow, "Continuous monitoring of intracranial pressure with a miniaturized fiber optic device," *J. Neurosurgery*, vol. 67, no. 2, pp. 206–209, 1987.

[7] J. S. Crutchfield, R. K. Narayan, C. S. Robertson, and L. H. Michael, "Evaluation of a fiber optic intracranial pressure monitor," *J. Neurosurgery*, vol. 72, no. 3 pp. 482–487, 1990.

[8] T. Sharma, S. S. Je, B. Gill, and J. X. J. Zhang, "Patterning piezoelectric thin film PVDF–TrFE based pressure sensor for catheter application," *Sens. Actuators A: Phys.*, vol. 177, pp. 87–92, 2012.

[9] C. Li, P. M. Wu, S. Lee, A. Gorton, M. J. Schulz, and C. H. Ahn, "Flexible dome and bump shape piezoelectric tactile sensors using PVDF-TrFE copolymer," *J. Microelectromech. Syst.*, vol. 17, no. 2, pp. 334–341, 2008.

[10] D. R. Bacon, "Characteristics of a PVDF membrane hydrophone for use in the range 1–100 MHz," *IEEE Trans. Sonics Ultrason.*, vol. SU-29, no. 1, pp. 18–25, Jan. 1982.

[11] P. E. Bloomfield, F. Castro, and R. Goeller, "The design, processing, evaluation and characterization of pyroelectric PVDF copolymer/silicon MOSFET detector arrays," in *Proc. 9th IEEE Int. Symp. Appl. Ferroelectr.*, 1991, pp. 725–728.

[12] J. Chang and L. Lin, "Large array electrospun PVDF nanogenerators on a flexible substrate," in *Proc. IEEE 16th Int. Solid-State Sens. Actuators Microsyst. Conf. (TRANSDUCERS)*, 2011, pp. 747–750.

[13] J. Dargahi, "A piezoelectric tactile sensor with three sensing elements for robotic, endoscopic and prosthetic applications," *Sens. Actuators A: Phys.*, vol. 80, no. 1, pp. 23–30, 2000.

[14] S. Kärki and J. Lekkala, "A new method to measure heart rate with EMFi and PVDF materials," *J. Med. Eng. Technol.*, vol. 33, no. 7 pp. 551–558, 2009.

[15] R. G. Kolkman, E. Hondebrink, W. Steenbergen, and F. F. Mul, "In vivo photoacoustic imaging of blood vessels using an extreme-narrow aperture sensor," *IEEE J. Select Topics Quantum Electron.*, vol. 9, no. 2, pp. 343–346, Mar./Apr. 2003.

[16] A. V. Shirinov and W. K. Schomburg, "Pressure sensor from a PVDF film," *Sens. Actuators A: Phys.*, vol. 142, no. 1, pp. 48–55, 2008.

[17] C. Chang, V. H. Tran, J. Wang, Y. K. Fuh and L. Lin "Direct-write piezoelectric polymeric nanogenerator with high energy conversion efficiency," *Nano Lett.*, vol. 10, no. 2, pp. 726–731, 2010.

[18] I. Clausen, S. T. Moe, L. G. W. Tvedt, A. Vogl, and D. T. Wang, "A miniaturized pressure sensor with inherent biofouling protection designed for in vivo applications," in *Proc. IEEE. Eng. Med. Biol. Soc. Annu. Int. Conf.*, 2011, pp. 1880–1883.

[19] B. J. Hansen, Y. Liu, R. Yang, and Z. L. Wang, "Hybrid nanogenerator for concurrently harvesting biomechanical and biochemical energy," *ACS Nano*, vol. 4, no. 7, pp. 3647–3652, 2010.
[20] P. Katta, M. Alessandro, R. D. Ramsier, and G. G. Chase "Continuous electrospinning of aligned polymer nanofibers onto a wire drum collector," *Nano Lett.*, vol. 4, no. 11, pp. 2215–2218, 2004.
[21] R. Tan, T. McClure, C. K. Lin, D. Jea, F. Dabiri, T. Massey, and J. Schmidt, "Development of a fully implantable wireless pressure monitoring system," *Biomed. Microdevices*, vol. 11, no. 1, pp. 259–264, 2009.
[22] C. Peng *et al.,* "A wireless and batteryless 130 mg 300 μW 10 b implantable blood-pressure-sensing microsystem for real-time genetically engineered mice monitoring," in *Proc. IEEE Int. Solid-State Circuits Conf. Digest Tech. Papers.*, 2009, pp. 428–429.
[23] W. Teo and S. Ramakrishna, "A review on electrospinning design and nanofibre assemblies," *Nanotechnology*, vol. 17, no. 14, p. R89, 2006.
[24] J. Doshi and D. H. Reneker, "Electrospinning process and applications of electrospun fibers," *J. Electrostatics*, vol. 35, no. 2, pp. 151–160, 1995.
[25] Z. M. Huang, Y. Z. Zhang, M. Kotaki, and S. Ramakrishna, "A review on polymer nanofibers by electrospinning and their applications in nanocomposites," *Composites Sci. Technol.*, vol. 63, no. 15, pp. 2223–2253, 2003.
[26] D. Li and Y. Xia, "Electrospinning of nanofibers: Reinventing the wheel?" *Adv. Mater.*, vol. 16, no. 14, pp. 1151–1170, 2004.
[27] J. Rafique, J. Yu, J. Yu, G. Fang, K. W. Wong, Z. Zheng, H. C. Ong and W. M. Lau., "Electrospinning highly aligned long polymer nanofibers on large scale by using a tip collector," *Appl. Phys. Lett.*, vol. 91, no. 6, pp. 063126-1–063126-3, 2007.
[28] S. H. Tan, R. Inai, M. Kotaki, and S. Ramakrishna, "Systematic parameter study for ultra-fine fiber fabrication via electrospinning process," *Polymer*, vol. 46, no. 16, pp. 6128–6134, 2005.
[29] D. H. Reneker and I. Chun, "Nanometre diameter fibres of polymer, produced by electrospinning," *Nanotechnology*, vol. 7, no. 3, p. 216, 1999.
[30] J. L. T. Sharma, S. Naik, K. Aroom, B. Gill, and J. X. J. Zhang, "Aligned electrospun PVDF-TrFE nanofibers for flexible pressure sensors on catheter," presented at the 17th Int. Conf. Solid-State Sens., Actuators Microsyst., Barcelona, Spain, 2013.
[31] T. Sharma, S. S. Je, B. Gill, and J. X. J. Zhang, "Patterning piezoelectric thin film PVDF–TrFE based pressure sensor for catheter application," *Sens. Actuators A: Phys.*, vol. 177, no. 0, pp. 87–92, 2012.
[32] C. E. Ayres, B. S. Jha, H. Meredith, J. R. Bowman, G. L. Bowlin, S. C. Henderson, and D. G. Simpso, "Measuring fiber alignment in electrospun scaffolds: A user's guide to the 2D fast Fourier transform approach," *J. Biomater. Sci. Polymer Edition*, vol. 19, no. 5, pp. 603–621, 2008.
[33] G. M. Kim, A. Wutzler, H. J. Radusch, G. H. Michler, P. Simon, R. A. Sperling, and W. J. Parak, "One-dimensional arrangement of gold nanoparticles by electrospinning," *Chem. Mater.*, vol. 17, no. 20, pp. 4949–4957, 2005.

Tushar Sharma received the B.Tech. degree in biotechnology from the Indian Institute of Technology Madras, Chennai, India, in 2008, and the M.S. and Ph.D. degrees in biomedical engineering from the University of Texas at Austin, USA, in 2010 and 2012.

He is currently with Intel Corporation, Hillsboro, OR, USA.

Dr. Tushar is the recipient of the following awards and honors Bhagyalakshmi and Krishna Iyengar award, special research grant, and Idea to Product—Texas and Global round winners.

Sahil Naik will be graduating from The University of Texas at Austin in May 2015 with a B.S. in Biomedical Engineering (Honors) and B.B.A. in Business Honors/Science and Technology Management.

Jewel Langevine is currently in the process of completing her bachelor's degree in Biomedical Engineering at The University of Texas at Austin in Austin, Texas, USA. She holds an associate's degree in Physical Science from San Jacinto College in Houston, Texas, USA. Jewel is completing a Business Foundations Certificate through the McCombs School of Business and an Elements of Computing Certificate from The University of Texas at Austin Department of Computer Science.

Brijesh Gill received the M.D. degree from The University of Alabama School of Medicine, Birmingham, AL, and the B.S. degree from Harvard University, Cambridge, MA.

He is currently a Trauma Surgeon and Associate Professor of Surgery at the University of Texas (UT) Health Medical School in Houston, USA. His current research interests include medical devices, cellular therapy, and tissue engineering.

John X. J. Zhang received the Ph.D. degree in electrical engineering from Stanford University, Stanford, CA, USA.

Dr. Zhang is a Professor at Thayer School of Engineering, Dartmouth College, NH, an Ivy League institution. Before joining Dartmouth, he was an Associate Professor with tenure in the Department of Biomedical Engineering at the University of Texas of Austin (UT Austin). He received his Ph.D. in Electrical Engineering from Stanford University and was a Research Scientist in Systems Biology at Massachusetts Institute of Technology (MIT). Zhang's research focuses on exploring bio-inspired nanomaterials, scale-dependent biophysics, and nanofabrication technology, towards developing new diagnostic devices and methods on probing complex cellular processes and biological networks critical to development and diseases.